instruments

MDPI

Article

Josephson Junctions as Single Microwave Photon Counters: Simulation and Characterization

Alessio Rettaroli [1,2,*], David Alesini [1], Danilo Babusci [1], Carlo Barone [3,4], Bruno Buonomo [1], Matteo Mario Beretta [1], Gabriella Castellano [5], Fabio Chiarello [1,5], Daniele Di Gioacchino [1], Giulietto Felici [1], Giovanni Filatrella [4,6], Luca Gennaro Foggetta [1], Alessandro Gallo [1], Claudio Gatti [1], Carlo Ligi [1], Giovanni Maccarrone [1], Francesco Mattioli [1,5], Sergio Pagano [3,4], Simone Tocci [1] and Guido Torrioli [1,5]

1 INFN, Laboratori Nazionali di Frascati, 00044 Frascati, Italy; david.alesini@lnf.infn.it (D.A.); danilo.babusci@lnf.infn.it (D.B.); bruno.buonomo@lnf.infn.it (B.B.); matteo.beretta@lnf.infn.it (M.M.B.); fabio.chiarello@ifn.cnr.it (F.C.); daniele.digioacchino@lnf.infn.it (D.D.G.); giulietto.felici@lnf.infn.it (G.F.); Luca.Foggetta@lnf.infn.it (L.G.F.); alessandro.gallo@lnf.infn.it (A.G.); claudio.gatti@lnf.infn.it (C.G.); carlo.ligi@lnf.infn.it (C.L.); giovanni.maccarrone@lnf.infn.it (G.M.); Francesco.mattioli@ifn.cnr.it (F.M.); simone.tocci@lnf.infn.it (S.T.); guido.torrioli@ifn.cnr.it (G.T.)
2 Dipartimento di Matematica e Fisica, Università di Roma Tre, 00154 Roma, Italy
3 Dipartimento di Fisica E.R. Caianiello, Università di Salerno, 84084 Fisciano, Italy; cbarone@unisa.it (C.B.); spagano@unisa.it (S.P.)
4 INFN, Gruppo Collegato di Salerno, 84084 Fisciano, Italy; filatrella@unisannio.it
5 Istituto di Fotonica e Nanotecnologie CNR, 00156 Roma, Italy; mariagabriella.castellano@cnr.it
6 Dipartimento di Scienze e Tecnologie, Università del Sannio, 82100 Benevento, Italy
* Correspondence: alessio.rettaroli@lnf.infn.it

Citation: Rettaroli, A.; Alesini, D.; Babusci, D.; Barone, C.; Buonomo, B.; Beretta, M.M.; Castellano, G.; Chiarello, F.; Di Gioacchino, D.; Felici, G.; et al. Josephson Junctions as Single Microwave Photon Counters: Simulation and Characterization. *Instruments* **2021**, *5*, 25. https://doi.org/10.3390/instruments5030025

Academic Editor: Andrea Messina

Received: 17 May 2021
Accepted: 12 July 2021
Published: 16 July 2021

Abstract: Detection of light dark matter, such as axion-like particles, puts stringent requirements on the efficiency and dark-count rates of microwave-photon detectors. The possibility of operating a current-biased Josephson junction as a single-microwave photon-detector was investigated through numerical simulations, and through an initial characterization of two Al junctions fabricated by shadow mask evaporation, done in a dilution refrigerator by measuring escape currents at different temperatures, from 40 mK up to the Al transition temperature. The escape dynamics of the junctions were reproduced in the simulation, including the dissipative effects. Inhibition of thermal activation was observed, leaving the macroscopic quantum tunneling as the dominant effect well beyond the crossover temperature.

Keywords: Josephson junction; axion; microwave

1. Introduction

1.1. Detection of Axions

In the 70s, an extension of the standard model of particle physics was advanced to explain the absence of CP violation in the strong interaction (strong CP problem) [1,2]. The theory predicts the existence of additional particles called axions [3,4]—sub-eV particles with feeble interactions with ordinary matter, which could be abundantly produced non-thermally in the early universe [5]. These characteristics make them good candidates for explaining the composition of cold dark matter (CDM) in the universe [6–8], an issue that modern cosmology and particle physics are still tackling.

Most of the experiments are sensitive to the axion–photon coupling constant $g_{a\gamma\gamma}$, which is proportional to the axion mass m_a. The region of interest for QCD axions is the yellow band in the m_a-$g_{a\gamma\gamma}$ plane shown in Figure 1.

Axions are an example of weakly interacting slim particles (WISPs), a category of particles emerging from many extensions of the standard model. WISPs as axion-like particles (ALPs) have a more general relationship between m_a and $g_{a\gamma\gamma}$.

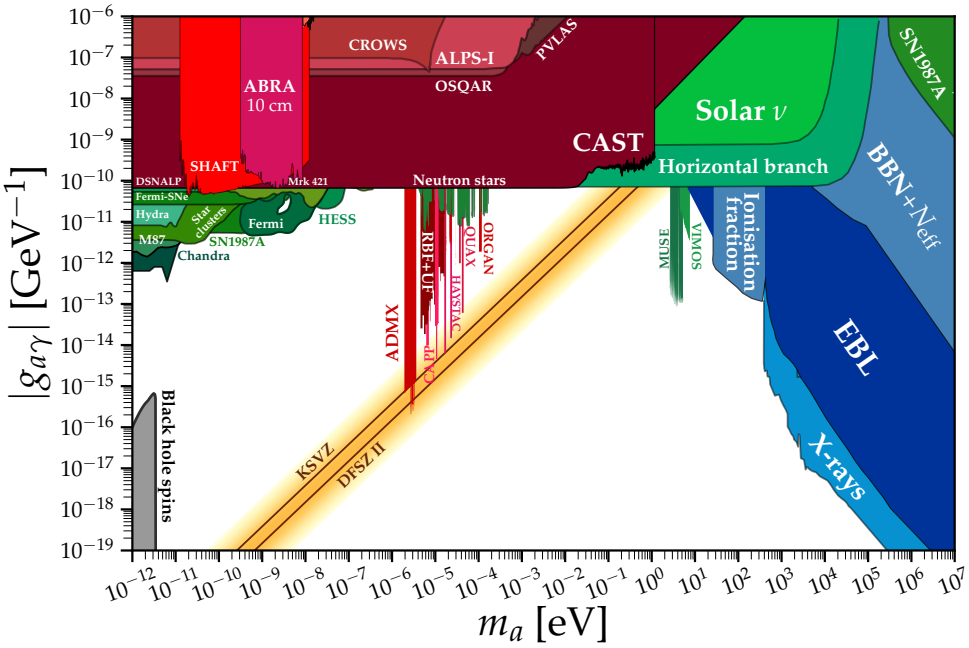

Figure 1. Axion parameter space showing the exclusion limits of experiments. The yellow band is representative of the QCD axions, together with the brown lines showing theoretical predictions of the KSVZ [9,10] and DFSZ [11,12] models. The plot is freely available from the online repository of [13].

The most exploited detection principle of axions and ALPs is the haloscope proposed by Sikivie [14,15], whose description is addressed in a review: [16]. Examples of running experiments, also shown by the vertical lines in Figure 1, are ADMX [17,18], HAYSTAC [19], CAPP-8T [20], CAPP-9T [21], ORGAN [22], and QUAX [23–26]; other proposed experiments include RADES [27,28], MADMAX [29], BRASS [30], and KLASH [31–33].

Since very tiny signals are involved in the game, searches of axions and ALPs will benefit from the latest developments in microwave quantum technologies, such as single microwave-photon detectors based on superconducting elements. In fact, as discussed in the next section, photon detectors may have better signal-to-noise ratios than quantum amplifiers, especially if they have low dark-count rates.

1.2. Single Photon Counters as Detectors

In the last two decades, attention to single photon detection has grown due to the demanding applications in quantum computing. Several techniques have been developed to detect single photons, such as quantum non-demolition measurements [34–39], switching detectors [40–42], hot electron detectors [43,44], and quantum dot detectors [45]. Belonging to switching detectors in the microwave range of radiation are Josephson junction (JJ)-based photon counters [41] and transmon qubits [35,46].

The best performances of currently running axion experiments were achieved with quantum-limited devices, such as superconducting quantum interference devices (SQUIDs) and Josephson parametric amplifiers (JPAs) [17–19,26,47], but efforts have been put toward counting single photons from axion interactions [42,46,48,49]. The reason is clear from [50]: working at higher frequencies while having a good scan rate at the same time requires single photon counters, which have better noise performances with respect to linear amplifiers above about 10 GHz. As discussed in [42], dark counts of single photon counters may be a limiting factor: in dark matter axion searches, a single photon counter will be competitive with a quantum-limited amplifier if the dark count ν_{dc} is below the intrinsic axion width $\Delta\nu_a \simeq \nu_a/10^6$ corresponding to 10 kHz at 10 GHz. Devices based on qubits have dark-counts rates $\nu_{dc} \sim p_{err}/t_{qubit}$ where $p_{err} \sim 10\%$ is a typical qubit readout error and $t_{qubit} \sim 10$ µs is a typical qubit decoherence time, corresponding to

$\nu_{dc} \sim 10$ kHz. On the contrary, switching devices, such as those based on current-biased Josephson junctions (CBJJ) [41,42,48], have the potential to reach dark counts at mHz rates. However, previous realization of a photon counter based on CBJJ [41] was operated in a regime with far higher dark counts, and no clear evidence exists that dark counts can be lowered without affecting the device efficiency. Within the SIMP project [51], we are developing a microwave single-photon detector based on CBJJ to couple to a haloscope, with the aim of probing the axion existence. In this paper we describe the device and its response to photon excitations obtained from simulations of different experimental conditions, showing that single photons can induce the switch of a JJ. We describe the first step in the characterization of a JJ with parameters optimized to detect photons originating from an axion conversion and derive the dark counts expected for a photon detector. We finally discuss the improvement needed to keep both high efficiency and a low dark-count rate.

2. A CBJJ as a Photon Detector

The electrodynamics of a CBJJ is accurately described in terms of the resistively shunted junction (*RSJ*) model [52], an equivalent electrical model whose circuit components are related to specific junction physical characteristics. With reference to Figure 2, the capacitor C_J represents the capacitance between the junction electrodes, the resistor R_J represents the tunneling of normal electrons (quasiparticles), and the component J_J represents the tunneling of superconductive electrons (Cooper pairs). The components I_s, I_b, and I_n represent current sources that will be detailed below. The current I_J through the component J_J and the corresponding voltage drop V_J are related to φ, the phase difference between the macroscopic wavefunctions of the two superconductors, by the Josephson equations:

$$I_J = I_0 \sin \varphi, \quad (1)$$

$$V_J = \frac{\hbar}{2e} \frac{d\varphi}{dt}. \quad (2)$$

I_0 is the maximum Cooper pair current that can flow through the J_J component, and $\hbar$ and e are the reduced Planck constant and electron charge, respectively. A stationary phase, and correspondingly, a zero average voltage is possible, according to the Josephson equations, Equations (1) and (2), when a dc current below I_0 flows in the J_J element. Depending on the values of the junction parameters (I_0, R_J, C_J), a finite-voltage state is also possible. If the dc bias current overcomes I_0, the phase cannot be stationary and a finite-voltage state is the only possibility. From the experimental point of view, this behavior is reflected in the occurrence of hysteresis in the current–voltage characteristic of the JJ, for certain dc bias current intervals, where two voltage states (zero and finite-valued) can be observed. Such hysteresis is at the basis of the use of a JJ as a detector. It is worth noting that in a typical tunnel-type JJ, the resistance of R_J strongly depends both on voltage and temperature. However, as the overall effect of the resistor is to introduce dissipation in the system, its nonlinearity is often not considered in the presence of moderate or weak damping. Another important effect of the quasiparticle current, modeled by R_J, is the presence of random charge fluctuations, which can be represented, using the fluctuation dissipation theorem, by a noise current source, indicated with I_n in Figure 2, whose spectral power density is assumed to be frequency independent (Johnson noise) [53].

In order to use a JJ as a detector, it is biased with a dc current just below I_0 through a suitable source, indicated with I_b in Figure 2. The occurrence of an external additional current (i.e., the signal to be detected) can induce the switching of the junction from the zero to the finite-voltage state. Of course, current noise can induce a switching, contributing to false alarms or dark counts in detector language. In the case of a simple CBJJ, the phase difference φ can be considered as a particle moving in a one-dimensional tilted cosine potential [54]; see Figure 3. The tilt of the potential corresponds to the normalized bias current flowing through the junction. The zero-voltage state corresponds to the confinement

of the particle in a potential well of barrier height ΔU [54], where it can oscillate at the characteristic plasma frequency, ω_J. Given enough energy, the particle can escape from this metastable state and roll down the potential slope, giving rise to a finite-voltage state [54]. At temperatures such that $k_B T \gg \hbar\omega_J$, the escape rate is dominated by the thermal activation (TA) process [55]:

$$\Gamma_T \sim \frac{\omega_J}{2\pi} \exp\left(-\frac{\Delta U}{k_B T}\right), \tag{3}$$

whereas at lower temperatures, it is dominated by macroscopic quantum tunneling (MQT) [55]:

$$\Gamma_q \sim \frac{\omega_J}{2\pi} \exp\left(-\frac{7.2\Delta U}{\hbar\omega_J}\right) \tag{4}$$

which provides an irreducible contribution to the dark-count rate.

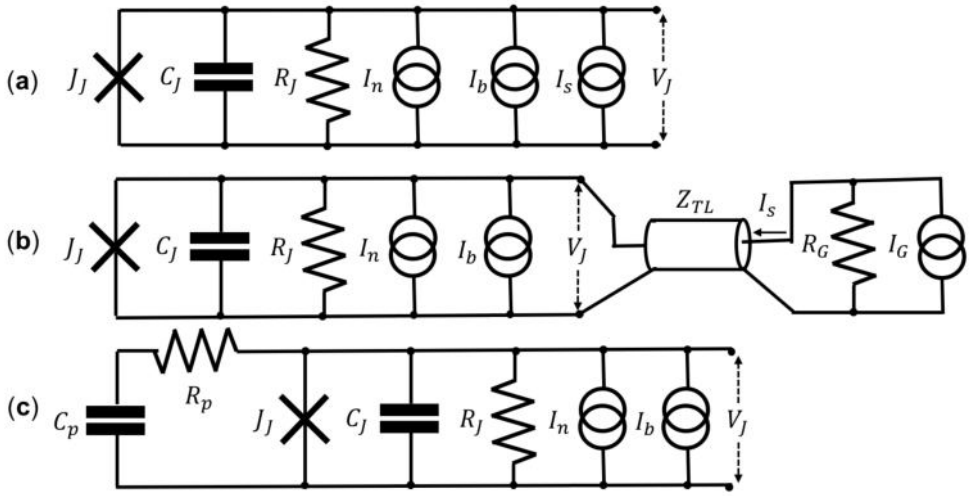

Figure 2. (**a**) An electrical model of a JJ with intrinsic and external current sources. (**b**) An electrical model of a JJ attached to a transmission line. (**c**) An electrical model of a JJ with a parasitic RC load.

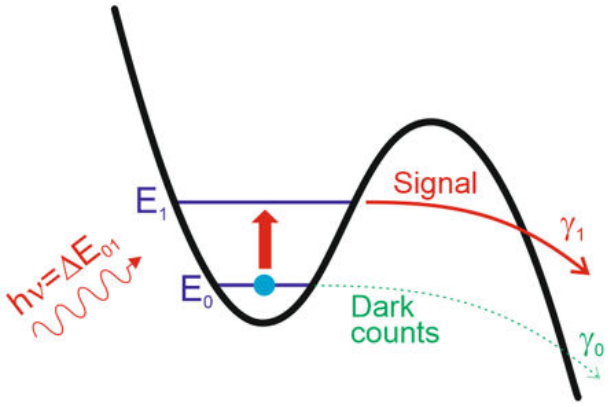

Figure 3. Equivalent potential of a JJ. The phase value is represented by the green particle which can overcame the energy barrier after the absorption of a suitable stimulus.

3. Device Simulation

We investigated the dynamics of a CBJJ in the presence of a microwave pulse, representing the process of single-photon absorption, by means of numerical simulations of the model equations [56]. We estimated in this way the parameters needed to make the junction switch in the presence of a signal.

3.1. Isolated CBJJ

To model a weak microwave field (weak because carrying few photons) coupled to the junction, we consider a deterministic current source, I_s in Figure 2, generating a properly shaped current pulse, representing the absorption of a single microwave photon. The following equations refer to the circuit of Figure 2a and describe the dynamics of an isolated junction where we imagine the current source directly coupled to the junction.

By denoting I_J as the current through the J_J element, I_{R_J} as the current through the resistor, and I_{C_J} as the current through the capacitor, we write the following current balance equation:

$$I_{C_J} + I_{R_J} + I_J = I_b + I_s(t) + I_n(t). \tag{5}$$

By using the constitutive relations of the resistor and capacitor, and the Josephson relations, we obtain the following second-order differential equation:

$$C_J \frac{\hbar}{2e} \frac{d^2\varphi}{dt^2} + \frac{1}{R_J} \frac{\hbar}{2e} \frac{d\varphi}{dt} + I_0 \sin\varphi = I_b + I_s(t) + I_n(t), \tag{6}$$

which, due to the presence of the stochastic noise term, is a Langevin equation [57]. By defining a normalized time $\tau = \omega_J t$, where

$$\omega_J = \sqrt{2eI_0/C_J\hbar} \tag{7}$$

is the Josephson plasma frequency, Equation (6) is re-written as:

$$\frac{d^2\varphi}{d\tau^2} + \alpha \frac{d\varphi}{d\tau} + \sin\varphi = \gamma_b + \gamma_s(\tau) + \gamma_n(\tau), \tag{8}$$

where the parameters are defined as

$$\alpha = \frac{1}{R_J C_J \omega_J}, \qquad \gamma_b = \frac{I_b}{I_0}, \qquad \gamma_s = \frac{I_s}{I_0}. \tag{9}$$

The statistical properties of the noise term γ_n are:

$$\begin{aligned} \langle \gamma_n(\tau) \rangle &= 0, \\ \langle \gamma_n(\tau), \gamma_n(\tau') \rangle &= 4D\delta(\tau - \tau'), \end{aligned} \tag{10}$$

where $D = k_B \mathcal{T} \omega_J / \left(R_J I_0^2\right)$ is the normalized noise intensity (k_B is the Boltzmann constant and $\mathcal{T}$ the physical temperature), $\delta()$ is the Dirac delta function, and the parentheses $\langle\,\rangle$ represent ensemble averages.

3.2. CBJJ Coupled to an RC Circuit

If the JJ is small in size, its capacitance and conductance can be very small too, thereby making it possible for external parasitic effects to modify its dynamics. To investigate these effects, we considered a model of a JJ loaded with a series parasitic RC circuit; see Figure 2c. In this case, Equation (5) becomes:

$$I_{C_J} + I_{R_J} + I_J + I_{R_p} = I_b + I_s(t) + I_n(t), \tag{11}$$

where I_{R_p} is the current flowing in the parasitic resistor R_p. The JJ voltage V_J is related to I_{R_p} by:

$$V_J = R_p I_{R_p} + \frac{1}{C_p} \int I_{R_p}\, dt. \tag{12}$$

By repeating the same procedure as before, we obtain the following two normalized differential equations:

$$\frac{d^2\varphi}{d\tau^2} + \alpha\frac{d\varphi}{d\tau} + \sin\varphi = \gamma_b + \gamma_s(\tau) + \gamma_n(\tau) + \gamma_R, \tag{13}$$

$$\frac{d\gamma_R}{d\tau} + \alpha_{RC}\gamma_R + \alpha_{int}\frac{d^2\varphi}{d\tau^2} = 0, \tag{14}$$

where

$$\alpha_{RC} = \frac{1}{R_p C_p \omega_J}, \qquad \alpha_{int} = \frac{1}{R_p C_J \omega_J}, \qquad \gamma_R = \frac{I_{R_p}}{I_0}. \tag{15}$$

3.3. CBJJ Coupled to a Transmission Line

The simplest design for a photon detector operating at microwave frequency based on a JJ is a transmission line (TL), such as a coplanar waveguide, terminated with a JJ. When the JJ is coupled to a TL with a characteristic impedance Z_{TL}, as shown in Figure 2b, signal reflection back to the TL has to be considered. The overall effect is modeled by a modified effective junction resistance, given by the values of the parallel resistors R_J and Z_{TL}. In Figure 2b, the current source I_s is given by an ideal generator I_g with an impedance R_g in parallel. The latter has to be equal to Z_{TL} to ensure impedance matching. To relate the simulation results to this particular case, we compare Equation (6) with the equation for the flux variable $\phi = \varphi(\phi_0/2\pi)$ in a TL terminated by a parallel LC (a linearized JJ) [58]:

$$C_J\ddot{\phi} + \frac{\phi}{L_J} + \frac{1}{Z_{TL}}\dot{\phi} = 2\frac{1}{Z_{TL}}\dot{\phi}^{in} = 2I^{in}, \tag{16}$$

where L_J is the Josephson inductance and the term $1/Z_{TL}$ models the aforementioned signal reflection on the TL. Moreover, the current I_s has to be interpreted as twice the input current I^{in}. The input peak-current due to a single photon on the waveguide with a Gaussian wavepacket of time duration σ_t is

$$I^2_{\text{peak}} = \frac{\hbar\omega_J}{Z_{TL}}\frac{2}{\sqrt{2\pi}\sigma_t}. \tag{17}$$

Then, the amplitude of the signal current I_s in Equation (6) corresponding to a single photon is:

$$I_s^{\text{photon}} = 2\sqrt{\frac{\hbar\omega_J}{Z_{TL}}\frac{2}{\sqrt{2\pi}\sigma_t}}. \tag{18}$$

For a 10 GHz photon with $\sigma_t = 600$ ps on a 50 Ω TL, this corresponds to about 26 nA.

We ran several simulations with the CBJJ either isolated or coupled to a TL excited by Gaussian current pulses of about 600 ps in length. We considered values of the critical current ranging from few hundred nanoamperes to a few microamperes, and junction capacitance ranging from a fraction of a picoFarad to a few picoFarads. The ratio I_b/I_0, about 0.8, was set in such a way as to keep the estimated rate of the MQT from the ground level by a few hertz at most. With the isolated junction we observed switching currents I_{switch} between 20 and 50 nA corresponding to about 1–4 photons, estimated as $N_\gamma = (I_{switch}/I_s^{\text{photon}})^2$. On the contrary, with the junction coupled to a 50 Ω TL, these values increased to a range between 200 to 300 nA corresponding to about 100 photons. The increase of number of photons is directly proportional to the relaxation rate of the junction $\gamma_{TL} = \omega_J/Q = \omega_J Z_J/Z_{TL} = 2\pi/Z_{TL}C_J$, where $Z_J = \sqrt{L_J/C_J}$, highlighting the need for a proper circuit for matching the CBJJ to the TL. Matching of a device to a TL is discussed in [39,59] where the detection efficiency is expressed as

$$P_{\text{R}} = \frac{4\gamma_{TL}\gamma_{\text{sw}}}{(\gamma_{TL} + \gamma_{\text{sw}})^2}. \tag{19}$$

γ_{sw} is the switching rate of the excited JJ to the resistive state. Perfect matching condition $\gamma_{TL} = \gamma_{sw}$ implies that the escape to the resistive state must be as fast as the relaxation of the junction to the ground level. This prevents us from using MQT transitions from the first excited level as a detection mechanism: an escape caused by MQT from the first excited level, E_1 in Figure 3, equal to $\gamma_{TL} \sim$ 1–10 GHz, would induce a dark-count rate due to escape from the ground level of about $\gamma_0 \sim 10^{-3}\gamma_{sw} \sim$ 1–10 MHz. On the contrary, while keeping low dark-count rates, two or more photons may induce the escape if absorbed by the junction within the relaxation time $1/\gamma_{TL}$.

4. Measurements

The study of the escape mechanisms of a CBJJ allow understanding and characterizing the escape rates in the absence of excitation signals, and therefore, of the dark counts. Much literature on measurements and interpretations of the escape processes has been published and underlines different dynamics, such as the TA regime, MQT, and phase diffusion (PD) with multiple retrapping processes [54,60–68]. The experimental conditions to highlight the diverse regimes and transitions between them have been defined. The regimes will depend on the comparison between the Josephson energies (E_J), related to the Josephson critical current I_0; the Coulomb energy E_C, depending on the capacity C_J; the plasma frequency ω_J proportional to $\sqrt{I_0/C_J}$ ratio; the quality factor $Q = \omega_J R_J C_J$, proportional to the losses; the potential tilt $E_J(I/I_0)$, controlled by the bias current I; and temperature [54,60–68]. This rich phenomenology of the escape process makes it ideal for a DC characterization of a JJ. In general, the typical escape dynamic's experimental setup consists of a slow ramping of the bias current across the junction up to the value of the critical current [61]. This ensures both that the JJ stays at the temperature of the cryostat thermal bath at milli-Kelvins, and that the superconducting state does not dissipate during the escape measurements before the final switching. Then, the data analyzed are the switching current distributions produced after countless repetitions of the process. Finally, measurements as a function of temperature can be a diagnostic tool for determining the processes of TA, tunneling, and phase diffusion regimes that regulate the escape process.

4.1. Fabrication Parameters from Simulations

The JJs we tested were fabricated at IFN-CNR by shadow mask evaporation (Figure 4), with electron beam lithography on a copolymer/PMMA bilayer (thickness of about 1 µm for each layer) over a Si substrate, with two evaporation angles of Al at 25° and 90° (thickness of about 30 nm), and with 5 min of oxidation at 5 mbar (expected thickness in the order of 1 nm). Junctions with different areas were fabricated: 2 µm × 2 µm ($I_0 \simeq$ 300 nA and $C \simeq$ 200 fF, expected from design parameters) and 2 µm × 4 µm ($I_0 \simeq$ 600 nA and $C \simeq$ 400 fF).

4.2. Setup

We tested the devices in a range of temperatures between 50 mK and about 1 K in a Leiden Cryogenics MCK 50–100 dilution refrigerator. We used a 4-terminal measurement scheme (Figure 5), with a bias resistance $R = 14.63$ kΩ at room temperature, twisted/shielded phosphor bronze cryogenic lines (about 25 Ω per line), and EMI low-pass filters at room temperature (bandpass 600 kHz). An Agilent 33220A waveform generator was used, together with two low noise preamplifiers EGG 5113 and a NI USB 6366 acquisition board.

This experimental setup allowed us to acquire current-voltage characteristics. We measured a gap $\Delta \simeq 200$ µV and critical currents within a factor 2 with respect to the estimated ones (Figure 6).

In order to measure the escape probabilities, we applied a sawtooth waveform with frequency $f = 314$ Hz, amplitude $I_{pp} = 670$ nA and offset $I_{off} = 250$ nA. In each period, during the slow growth (with slope $dI/dt = 210$ µA/s), sudden transition to the voltage state occurred at random values of current I_c. In the fast decrease region, the junction

resets to the superconducting state. We acquired a series of $N = 5000$ transition values I_c by using the voltage jumps as trigger signals. These values were arranged in a histogram to evaluate the escape probability $P(I)$. In Figure 7 we report the experimental escape probabilities at different temperatures ranging from about 40 to 850 mK. Data analysis is discussed in the next section.

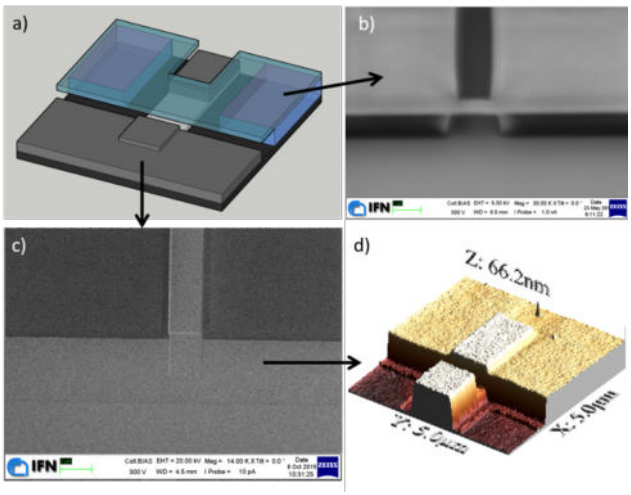

Figure 4. (**a**) Schematic image of the shadow mask evaporation technique. The copolymer/PMMA bilayer was exposed by EBL and developed, in order to obtain a self-standing bridge of the desired geometry, as shown by the scanning electron microscope (SEM) micrograph in (**b**). A two-angle evaporation with an oxidation step in between defines the junction geometry (light and dark gray in (**a**). (**c**) SEM micrograph of the junction after the lift-off process used to remove the bilayer mask. (**d**) An atomic force microscope (AFM) characterization of a typical junction.

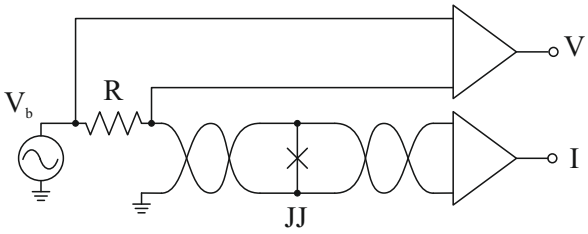

Figure 5. A scheme of the experimental setup.

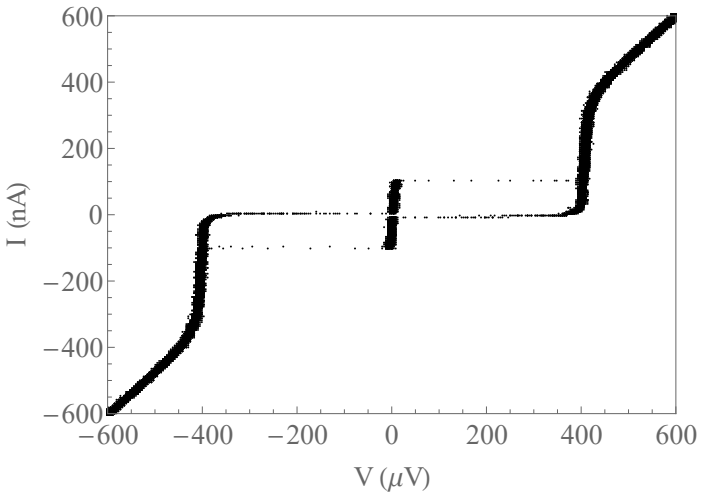

Figure 6. Measured voltage-current characteristic of a Josephson junction (2 µm× 2 µm).

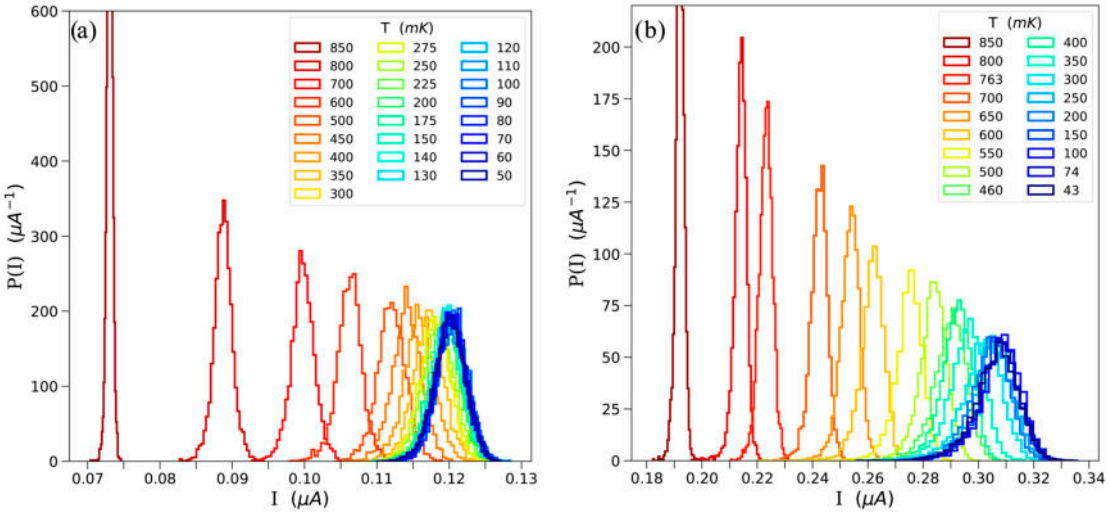

Figure 7. Filtered escape current distributions for 2 μm × 2 μm junction (**a**) and for 2 μm × 4 μm junction (**b**). The ranges of temperatures are slightly different and are shown in the legends. Rightmost curves are taken at the lowest temperature and leftmost curves are taken at highest temperature. The effect of the filter was a reduction of σ up to 20% with respect to the unfiltered data (not shown); $\langle I_c \rangle$ was left unchanged.

5. Results and Discussion

5.1. Results

From the 5000 transition values I_c we constructed escape-probability densities. Before doing this, we applied a fast Fourier transform to the measured I_c series and identified a narrow peak at 100 Hz and minor peaks at lower frequencies, attributed to electronic noise in the current-measurement setup. We calculated the peaks' frequencies, phases, and amplitudes from the Fourier analysis, and filtered out the noise from the original I_c series. We thereby obtained a 20% improvement in resolution. We show the experimental switching distributions $P(I)$ obtained after filtering the data for each temperature in Figure 7a,b—the smallest and the largest junctions, respectively.

We extracted the mean $\langle I_c \rangle$ and width σ from each distribution as an arithmetic mean and a standard deviation. These are plotted as a function of temperature in Figure 8a,b, for the two junctions.

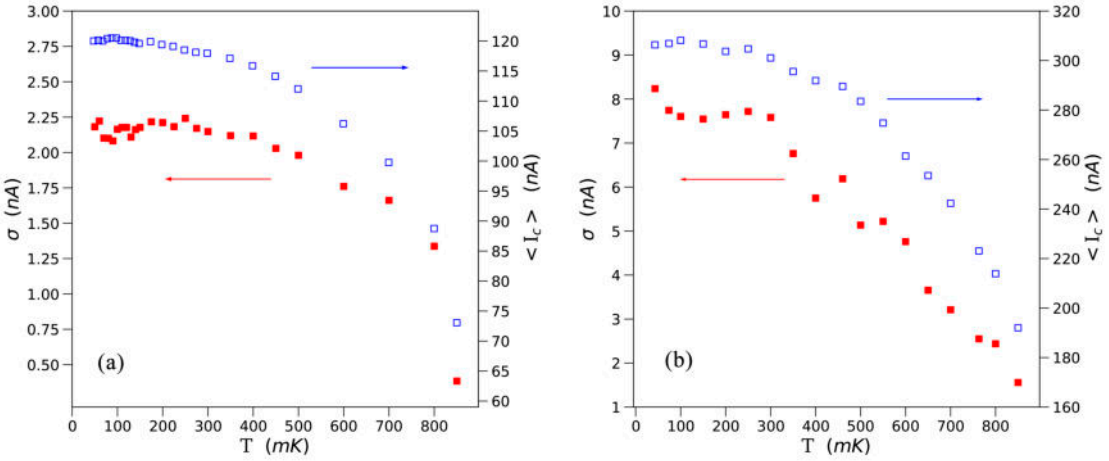

Figure 8. $\langle I_c \rangle$ and σ for 2 μm × 2 μm junction (**a**) and for 2 μm × 4 μm junction (**b**). In both plots, the red squares are relative to the left axis (widths) and the empty blue squares are relative to the right axis (mean currents), as indicated by the arrows.

The mean critical current values (empty blue squares) follow qualitatively the typical BCS behavior [52] as a function of temperature. The widths (full red squares) present a peculiar feature. The constant behavior of σ at low temperatures was expected from

quantum tunneling processes (Equation (4)), whereas its decrease at higher temperatures, above about 400 mK, suggests that TA (Equation (3)) is suppressed. We attribute the decreasing regime partially to the decrease of the critical current with increasing temperature, although a further contribution due to retrapping is not excluded.

5.2. Interpretations of Results

To investigate the effect of a dissipative environment on the escape by TA, we ran simulations of the JJ in parallel to the dissipative RC circuit shown in Figure 2c and described in Section 3.2. In our experimental setup, the parasitic circuit is represented by the dc lines carrying the bias current to the junction. The driving equations of the simulations were obtained from Equations (11)–(15) by setting the current source $I_s(t)$ to zero. Qualitatively, in the RCSJ model, energy dissipation induced a relaxation rate

$$\Gamma_{\text{rel}} = \frac{1}{\tau} = \frac{1}{RC_J} = \frac{\omega_J}{Q}, \tag{20}$$

where R is the parallel between R_J and R_p. If relaxation is faster than the TA, the latter is suppressed:

$$\frac{\omega_J}{2\pi} \exp\left(-\frac{\Delta U}{k_B T}\right) < \frac{\omega_J}{Q}, \tag{21}$$

corresponding to the condition

$$R < 2\pi Z_J \exp\left(\frac{\Delta U}{k_B T}\right). \tag{22}$$

Thus, even for temperatures such that $k_B T \sim \Delta U$, TA is suppressed if $R < 2\pi e Z_J \sim 20 Z_J$. For the described junction, Z_J is $\sim 50\Omega$; therefore, an external resistance equal to about 1 kΩ would dominate in parallel to $R_J = 100$ kΩ, causing dissipation. On the contrary, the MQT process, which is not affected by dissipation, would become the dominant switching effect even at temperatures higher than the expected crossing temperature. This was confirmed by our simulations, whose results for different simulation parameters are shown in Figure 9. The inclusion of the RC circuit strongly modifies the qualitative behavior of I_c and σ as a function of the temperature. In Figure 10 we show the comparison of the experimental results obtained for the 2 µm × 2 µm junction and results of a simulation run with parameters $I_0 = 143$ nA, $C_J = 0.2$ pF, $R_J = 100$ kΩ, $C = 2$ pF, and $R_p = 1$ kΩ, where only MQT and dissipation were included. Both the simulated distributions of I_c and σ are in good agreement with the measured ones. As anticipated, a further contribution from a retrapping process at a higher temperature could take into account the observed residual difference between the experimental and simulated values of σ.

5.3. Dark-Count Rate

Finally, we investigate the dark-count rate performances of the 2 µm × 2 µm junction to predict how it would behave if used as a single photon counter. Following [69], we calculated the escape rate from the current distribution of the JJ taken at the lowest temperature (50 mK). The result as a function of the bias current is shown in Figure 11, where the blue dots represent the escape rate values extracted from data. The dashed red line is the escape rate expected from MQT only. It reproduced the data for currents up to 120 nA, where the current distribution at 50 mK has its maximum (Figure 7a). The deviation at higher currents is attributable to a Gaussian resolution effect with standard deviation $\sigma = 1.1$ nA, as confirmed by the data's agreement with the green solid line obtained by applying such a smearing to the theoretical current distribution of the MQT before deriving the escape rate.

To determine the working point for a photon detector based on a similar JJ ($I_0 = 140$ nA, $C_J = 0.2$ pF), we relied on the simulation of an "isolated" junction with $R_J = 5$ kΩ driven by a resonant rf Gaussian pulse of frequency 6.5 GHz, duration $\sigma_t = 370$ ps, and peak current $I_{max} = 21$ nA corresponding to one photon. The simulated

junction switched for a bias current $I_b \simeq 91$ nA ($\gamma_b \simeq 0.65$) when the junction plasma frequency was about 6.5 GHz. By extrapolating the escape rate measured in our data (Figure 11) to the value $\gamma_b \simeq 0.65$, we estimated for the photon detector a dark-count rate of about 1 mHz.

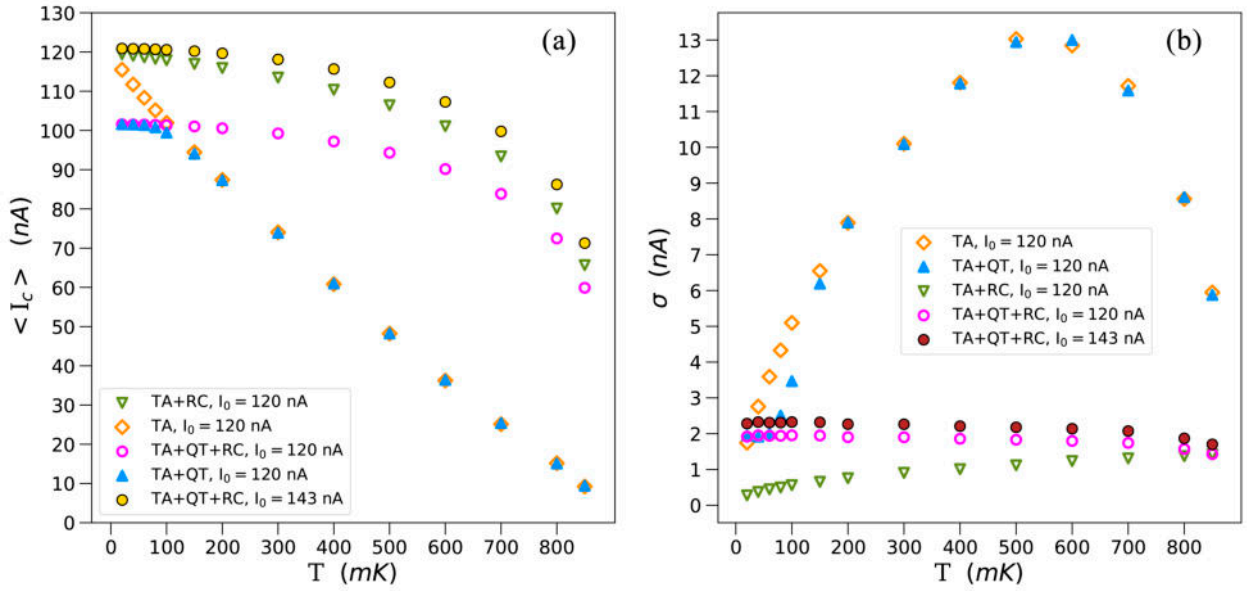

Figure 9. Mean switching currents (**a**) and widths (**b**) of the simulated data for different simulation parameters. In the legend, TA refers to thermal activation processes, QT to quantum tunneling, and RC to the dissipation effect due to the external circuit.

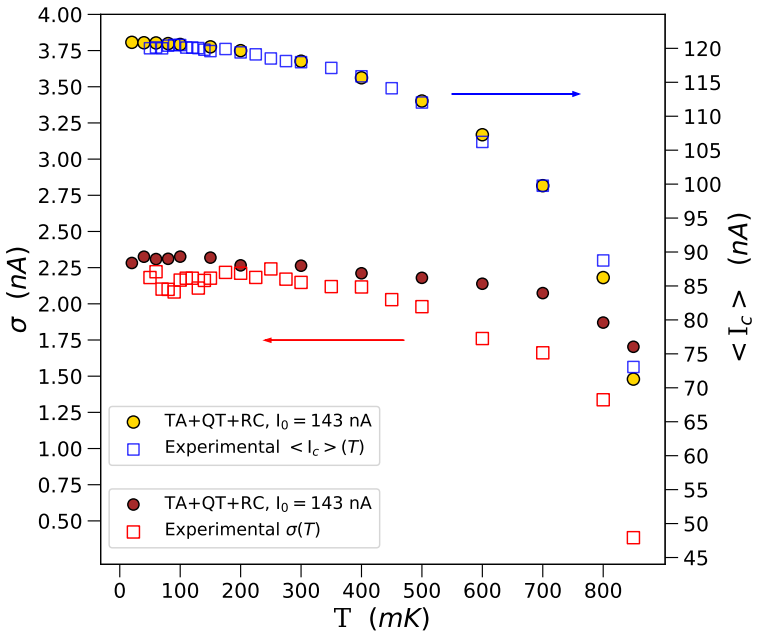

Figure 10. Comparison of the mean switching currents and widths of the simulated data with $R_p = 1$ kΩ, $C = 2$ pF, $R_J = 100$ kΩ, $I_0 = 143$ nA, and $C_J = 0.2$ pF with respect to experimental results of the 2 μm × 2 μm junction, shown in empty squares.

It should be noted that in simulations with $R_J < 1.5$ kΩ, dissipation inhibits junction switches, as observed in the TA process in our data and as expected from the discussion in Section 5.2. As already noted in Section 3.3, when a junction is coupled to a TL, the 50 Ω line impedance acts as a dissipative medium, preventing the junction from switching. Finally, when $\gamma_b \simeq 0.65$, the height of the potential well is estimated to be 28 GHz, corresponding to

about four energy levels, showing that the current pulse must induce a strong modification of the potential to cause the junction switch.

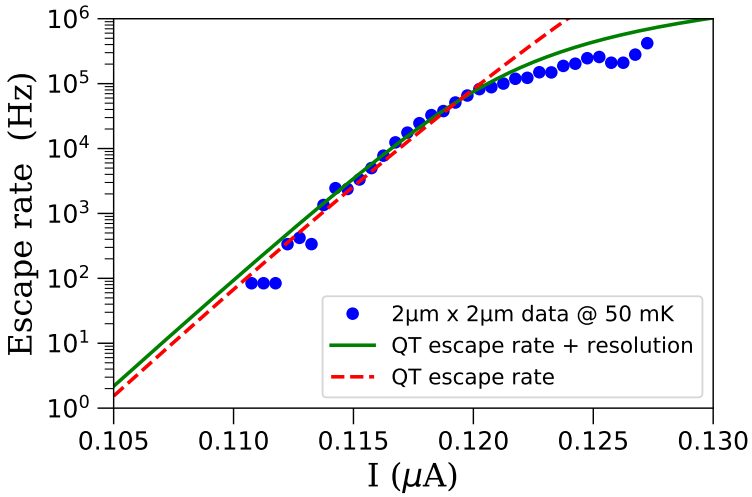

Figure 11. Experimental dark-count rate for the 2 µm × 2 µm junction at 50 mK, compared with quantum tunneling escape rate (red dashed line) and quantum tunneling plus the effect of 1.1 nA of Gaussian smearing (green solid line).

6. Conclusions

We have investigated the escape mechanism of a CBJJ both with simulations and through measurements of the escape currents in two Al JJs. We highlighted the effect of the dissipative mechanism introduced by the current leads—in particular, the suppression of escape induced by TA. While this suppression leads to a reduction in the escape rates and to dark counts above the crossover temperature, it also implies a low quality factor with consecutive reductions in signal efficiency, and this must be taken into account in the design of a microwave photon counter. We in fact showed with simulations that a current pulse with peak current $I_{max} = 21$ nA, corresponding to a single photon, induces the switch of an isolated junction of critical current $I_0 = 140$ nA when biased with a current $I_b \simeq 91$ nA, and that the expected dark-count rate would be at the mHz-level. This value was confirmed by the escape rates extracted from our data. However, when the junction was not isolated but coupled to a TL, the simulation showed that switches were inhibited, and larger current pulses were required. The JJ must then be resonantly matched with the TL with a bandwith estimated to be in the order of $1/R_jC_j \sim 1$ GHz.

Author Contributions: Formal analysis, A.R., C.B., F.C., D.D.G., G.F. (Giovanni Filatrella), C.G., C.L., G.M., S.P. and S.T.; investigation, A.R., D.A., D.B., B.B., M.M.B., G.C., F.C., D.D.G., G.F. (Giulietto Felici), L.G.F., A.G., C.G., C.L., G.M., F.M., S.P., S.T. and G.T.; resources, G.C., F.C., F.M. and G.T.; software, C.B., F.C., G.F. (Giovanni Filatrella) and S.P.; supervision, C.G.; writing—original draft, A.R., F.C., D.D.G., C.G., C.L., F.M. and S.P. All authors have read and agreed to the published version of the manuscript.

Funding: This research received no external funding.

Acknowledgments: We are grateful to G. Papalino and M. Iannarelli (LNF) for help with electronics and F. Tabacchioni (INAF) for cryogenics support. We would like to thank also A. Tudorache for his help during the short time spent at LNF.

Conflicts of Interest: The authors declare no conflict of interest.

References

1. Peccei, R.D.; Quinn, H.R. CP Conservation in the Presence of Pseudoparticles. *Phys. Rev. Lett.* **1977**, *38*, 1440–1443. [CrossRef]
2. Peccei, R.D.; Quinn, H.R. Constraints imposed by CP conservation in the presence of pseudoparticles. *Phys. Rev. D* **1977**, *16*, 1791–1797. [CrossRef]

3. Weinberg, S. A New Light Boson? *Phys. Rev. Lett.* **1978**, *40*, 223–226. [CrossRef]
4. Wilczek, F. Problem of Strong *P* and *T* Invariance in the Presence of Instantons. *Phys. Rev. Lett.* **1978**, *40*, 279–282. [CrossRef]
5. Sikivie, P., Axions. In *Particle Dark Matter: Observations, Models and Searches*; Bertone, G., Ed.; Cambridge University Press: Cambridge, UK, 2010.
6. Preskill, J.; Wise, M.B.; Wilczek, F. Cosmology of the invisible axion. *Phys. Lett. B* **1983**, *120*, 127–132. [CrossRef]
7. Abbott, L.; Sikivie, P. A cosmological bound on the invisible axion. *Phys. Lett. B* **1983**, *120*, 133–136. [CrossRef]
8. Dine, M.; Fischler, W. The not-so-harmless axion. *Phys. Lett. B* **1983**, *120*, 137–141. [CrossRef]
9. Kim, J.E. Weak-Interaction Singlet and Strong CP Invariance. *Phys. Rev. Lett.* **1979**, *43*, 103–107. [CrossRef]
10. Shifman, M.A.; Vainshtein, A.I.; Zakharov, V.I. Can confinement ensure natural CP invariance of strong interactions? *Nucl. Phys. B* **1980**, *166*, 493–506. [CrossRef]
11. Dine, M.; Fischler, W.; Srednicki, M. A simple solution to the strong CP problem with a harmless axion. *Phys. Lett. B* **1981**, *104*, 199–202. [CrossRef]
12. Zhitnitsky, A.R. On Possible Suppression of the Axion Hadron Interactions. (In Russian). *Sov. J. Nucl. Phys.* **1980**, *31*, 260.
13. O'Hare, C. cajohare/AxionLimits: AxionLimits. **2020**, Available online: https://zenodo.org/record/3932430#.YO-ZTPkzZPY (accessed on 15 July 2021).
14. Sikivie, P. Experimental Tests of the "Invisible" Axion. *Phys. Rev. Lett.* **1983**, *51*, 1415–1417. [CrossRef]
15. Sikivie, P. Detection rates for "invisible"-axion searches. *Phys. Rev. D* **1985**, *32*, 2988–2991. [CrossRef]
16. Irastorza, I.G.; Redondo, J. New experimental approaches in the search for axion-like particles. *Prog. Part Nucl. Phys.* **2018**, *102*, 89–159. [CrossRef]
17. Du, N.; Force, N.; Khatiwada, R.; Lentz, E.; Ottens, R.; Rosenberg, L.J.; Rybka, G.; Carosi, G.; Woollett, N.; Bowring, D.; et al. Search for Invisible Axion Dark Matter with the Axion Dark Matter Experiment. *Phys. Rev. Lett.* **2018**, *120*, 151301. [CrossRef]
18. Braine, T.; Cervantes, R.; Crisosto, N.; Du, N.; Kimes, S.; Rosenberg, L.J.; Rybka, G.; Yang, J.; Bowring, D.; Chou, A.S.; et al. Extended Search for the Invisible Axion with the Axion Dark Matter Experiment. *Phys. Rev. Lett.* **2020**, *124*, 101303. [CrossRef]
19. Backes, K.M.; Palken, D.A.; Al Kenany, S.; Brubaker, B.M.; Cahn, S.B.; Droster, A.; Hilton, G.C.; Ghosh, S.; Jackson, H.; Lamoreaux, S.K.; et al. A quantum enhanced search for dark matter axions. *Nature* **2021**, *590*, 238. [CrossRef]
20. Choi, J.; Ahn, S.; Ko, B.; Lee, S.; Semertzidis, Y. CAPP-8TB: Axion Dark Matter Search Experiment around 6.7 μeV. *arXiv* **2020**, arXiv:2007.07468.
21. Jeong, J.; Youn, S.; Bae, S.; Kim, J.; Seong, T.; Kim, J.E.; Semertzidis, Y.K. Search for Invisible Axion Dark Matter with a Multiple-Cell Haloscope. *Phys. Rev. Lett.* **2020**, *125*, 221302. [CrossRef] [PubMed]
22. McAllister, B.T.; Flower, G.; Ivanov, E.N.; Goryachev, M.; Bourhill, J.; Tobar, M.E. The ORGAN experiment: An axion haloscope above 15 GHz. *Phys. Dark Universe* **2017**, *18*, 67–72. [CrossRef]
23. Crescini, N.; Alesini, D.; Braggio, C.; Carugno, G.; Di Gioacchino, D.; Gallo, C.S.; Gambardella, U.; Gatti, C.; Iannone, G.; Lamanna, G.; et al. Operation A Ferromagn. Axion Haloscope $m_a = 58$ μeV. *Eur. Phys. J. C* **2018**, *78*, 703. [CrossRef]
24. Crescini, N.; Alesini, D.; Braggio, C.; Carugno, G.; D'Agostino, D.; Di Gioacchino, D.; Falferi, P.; Gambardella, U.; Gatti, C.; Iannone, G.; et al. Axion Search with a Quantum-Limited Ferromagnetic Haloscope. *Phys. Rev. Lett.* **2020**, *124*, 171801. [CrossRef]
25. Alesini, D.; Braggio, C.; Carugno, G.; Crescini, N.; D'Agostino, D.; Di Gioacchino, D.; Di Vora, R.; Falferi, P.; Gallo, S.; Gambardella, U.; et al. Galactic axions search with a superconducting resonant cavity. *Phys. Rev. D* **2019**, *99*, 101101. [CrossRef]
26. Alesini, D.; Braggio, C.; Carugno, G.; Crescini, N.; D'Agostino, D.; Di Gioacchino, D.; Di Vora, R.; Falferi, P.; Gambardella, U.; Gatti, C.; et al. Search for invisible axion dark matter of mass $m_a = 43$ μeV with the QUAX–$a\gamma$ experiment. *Phys. Rev. D* **2021**, *103*, 102004. [CrossRef]
27. Melcón, A.Á.; Cuendis, S.A.; Cogollos, C.; Díaz-Morcillo, A.; Döbrich, B.; Gallego, J.D.; Gimeno, B.; Irastorza, I.G.; Lozano-Guerrero, A.J.; Malbrunot, C.; et al. Axion searches with microwave filters: The RADES project. *J. Cosmol. Astropart. Phys.* **2018**, *2018*, 040. [CrossRef]
28. Arguedas, Cuendis, S.; Álvarez, Melcón, A.; Cogollos, C.; Díaz-Morcillo, A.; Döbrich, B.; Gallego, J.D.; Gimeno, B.; Irastorza, I.G.; Lozano-Guerrero, A.J.; Malbrunot, C.; et al. The 3 cavity prototypes of RADES, an axion detector using microwave filters at CAST. *arXiv* **2019**, arXiv:1903.04323.
29. Caldwell, A.; Dvali, G.; Majorovits, B.; Millar, A.; Raffelt, G.; Redondo, J.; Reimann, O.; Simon, F.; Steffen, F. Dielectric Haloscopes: A New Way to Detect Axion Dark Matter. *Phys. Rev. Lett.* **2017**, *118*, 091801. [CrossRef]
30. BRASS: Broadband Radiometric Axion SearcheS. Available online: http://www.iexp.uni-hamburg.de/groups/astroparticle/brass/brassweb.htm (accessed on 15 July 2021).
31. Alesini, D.; Babusci, D.; Di Gioacchino, D.; Gatti, C.; Lamanna, G.; Ligi, C. The KLASH Proposal. *arXiv* **2017**, arXiv:1707.06010.
32. Gatti, C.; Alesini, D.; Babusci, D.; Braggio, C.; Carugno, G.; Crescini, N.; Di Gioacchino, D.; Falferi, P.; Lamanna, G.; Ligi, C.; et al. The Klash Proposal: Status and Perspectives. In Proceedings of the 14th Patras Workshop on Axions, WIMPs and WISPs (AXION-WIMP 2018) (PATRAS 2018), Hamburg, Germany, 18–22 June 2018
33. Alesini, D.; Babusci, D.; Björkeroth, F.; Bossi, F.; Ciambrone, P.; Monache, G.D.; Di Gioacchino, D.; Falferi, P.; Gallo, A.; Gatti, C.; et al. KLASH Conceptual Design Report. *arXiv* **2019**, arXiv:1911.02427.
34. Gleyzes, S.; Kuhr, S.; Guerlin, C.; Bernu, J.; Deleglise, S.; Hoff, U.B.; Brune, M.; Raimond, J.-M.; Haroche, S. Quantum jumps of light recording the birth and death of a photon in a cavity. *Nature* **2007**, *446*, 297–300. [CrossRef]

35. Schuster, D.I.; Houck, A.A.; Schreiner, J.A.; Wallraff, A.; Gambetta, J.M.; Blais, A.; Frunzion, A.; Majer, J.; Johnson, B.; Devoret, H.; et al. Resolving photon number states in a superconducting circuit. *Nature* **2007**, *445*, 515–518. [CrossRef]
36. Johnson, B.R.; Reed, M.D.; Houck, A.A.; Schuster, D.I.; Bishop, L.S.; Ginossar, E.; Gambetta, J.M.; DiCarlo, L.; Frunzio, L.; Girvin, S.M.; et al. Quantum Non-Demolition Detection Single Microwave Photons A Circuit. *Nat. Phys.* **2010**, *6*, 663–667. [CrossRef]
37. Besse, J.C.; Gasparinetti, S.; Collodo, M.C.; Walter, T.; Kurpiers, P.; Pechal, M.; Eichler, C.; Wallraff, A. Single-Shot Quantum Nondemolition Detection of Individual Itinerant Microwave Photons. *Phys. Rev. X* **2018**, *8*, 021003. [CrossRef]
38. Kono, S.; Koshino, K.; Tabuchi, Y.; Noguchi, A.; Nakamura, Y. Quantum non-demolition detection of an itinerant microwave photon. *Nat. Phys.* **2018**, *14*, 546–549. [CrossRef]
39. Lescanne, R.; Deléglise, S.; Albertinale, E.; Réglade, U.; Capelle, T.; Ivanov, E.; Jacqmin, T.; Leghtas, Z.; Flurin, E. Irreversible Qubit-Photon Coupling for the Detection of Itinerant Microwave Photons. *Phys. Rev. X* **2020**, *10*, 021038. [CrossRef]
40. Inomata, K.; Lin, Z.; Koshino, K.; Oliver, W.D.; Tsai, J.-S.; Yamamoto, T.; Nakamura, Y. Single microwave-photon detector using an artificial Λ-type three-level system. *Nat. Commun.* **2016**, *7*, 1–7. [CrossRef] [PubMed]
41. Chen, Y.F.; Hover, D.; Sendelbach, S.; Maurer, L.; Merkel, S.T.; Pritchett, E.J.; Wilhelm, F.K.; McDermott, R. Microwave Photon Counter Based on Josephson Junctions. *Phys. Rev. Lett.* **2011**, *107*, 217401. [CrossRef] [PubMed]
42. Kuzmin, L.S.; Sobolev, A.S.; Gatti, C.; Di Gioacchino, D.; Crescini, N.; Gordeeva, A.; Il'ichev, E. Single Photon Counter Based on a Josephson Junction at 14 GHz for Searching Galactic Axions. *IEEE Trans. Appl. Supercond.* **2018**, *28*, 1–5. [CrossRef]
43. Semenov, A.D.; Gol'tsman, G.N.; Sobolewski, R. Hot-electron effect in superconductors and its applications for radiation sensors. *Supercond. Sci. Technol.* **2002**, *15*. [CrossRef]
44. Paolucci, F.; Buccheri, V.; Germanese, G.; Ligato, N.; Paoletti, R.; Signorelli, G.; Bitossi, M.; Spagnolo, P.; Falferi, P.; Rajteri, M.; et al. Development of highly sensitive nanoscale transition edge sensors for gigahertz astronomy and dark matter search. *J. Appl. Phys.* **2020**, *128*, 194502. [CrossRef]
45. Komiyama, S. Single-Photon Detectors in the Terahertz Range. *IEEE J. Sel. Top. Quantum Electron.* **2011**, *17*, 54–66. [CrossRef]
46. Dixit, A.V.; Chakram, S.; He, K.; Agrawal, A.; Naik, R.K.; Schuster, D.I.; Chou, A. Searching for Dark Matter with a Superconducting Qubit. *Phys. Rev. Lett.* **2021**, *126*, 141302. [CrossRef] [PubMed]
47. Kutlu, Ç.; van Loo, A.F.; Uchaikin, S.V.; Matlashov, A.N.; Lee, D.; Oh, S.; Kim, J.; Chung, W.; Nakamura, Y.; Semertzidis, Y.K. Characterization of a flux-driven Josephson parametric amplifier with near quantum-limited added noise for axion search experiments. *Supercond. Sci. Technol.* **2021**. [CrossRef]
48. Revin, L.S.; Pankratov, A.L.; Gordeeva, A.V.; Yablokov, A.A.; Rakut, I.V.; Zbrozhek, V.O.; Kuzmin, L.S. Microwave photon detection by an Al Josephson junction. *Beilstein J. Nanotechnol.* **2020**, *11*, 960–965. [CrossRef] [PubMed]
49. Alesini, D.; Babusci, D.; Barone, C.; Buonomo, B.; Beretta, M.M.; Bianchini, L.; Castellano, G.; Chiarello, F.; Di Gioacchino, D.; Falferi, P.; et al. Development of a Josephson junction based single photon microwave detector for axion detection experiments. *J. Phys. Conf. Ser.* **2020**, *1559*, 012020. [CrossRef]
50. Lamoreaux, S.K.; van Bibber, K.A.; Lehnert, K.W.; Carosi, G. Analysis of single-photon and linear amplifier detectors for microwave cavity dark matter axion searches. *Phys. Rev. D* **2013**, *88*, 035020. [CrossRef]
51. Alesini, D.; Babusci, D.; Barone, C.; Buonomo, B.; Beretta, M.M.; Bianchini, L.; Castellano, G.; Chiarello, F.; Di Gioacchino, D.; Falferi, P.; et al. Status of the SIMP Project: Toward the Single Microwave Photon Detection. *J. Low Temp. Phys.* **2020**, *199*, 348–354. [CrossRef]
52. Barone, A.; Paternò, G. *Physics and Applications of the Josephson Effect*; Wiley: New York, NY, USA, 1982.
53. Kogan, S. *Electronic Noise and Fluctuations in Solids*; Cambridge University Press: Cambridge, UK, 1996.
54. Martinis, J.M.; Devoret, M.H.; Clarke, J. Energy-Level Quantization in the Zero-Voltage State of a Current-Biased Josephson Junction. *Phys. Rev. Lett.* **1985**, *55*, 1543–1546. [CrossRef]
55. Devoret, M.H.; Martinis, J.M.; Clarke, J. Measurement of Macroscopic Quantum Tunneling out of the Zero-Voltage State of a Current-Biased Josephson Junction. *Phys. Rev. Lett.* **1985**, *55*, 1908. [CrossRef] [PubMed]
56. Piedjou Komnang, A.; Guarcello, C.; Barone, C.; Gatti, C.; Pagano, S.; Pierro, V.; Rettaroli, A.; Filatrella, G. Analysis of Josephson junctions switching time distributions for the detection of single microwave photons. *Chaos Solitons Fractals* **2020**, *142*, 110496. [CrossRef]
57. Ben-Jacob, E.; Bergman, D. Thermal noise effects on the microwave-induced steps of a current-driven josephson junction. *Phys. Rev. A* **1984**, *29*, 2021–2028. [CrossRef]
58. Yurke, B.; Denker, J. Quantum Network Theory. *Phys. Rev. A* **1984**, *29*, 1419. [CrossRef]
59. Schondorf, M.; Govia, L.; Vavilov, M.; McDermott, R.; Wilhelm, F. Optimizing microwave photodetection: Input—Output theory. *Quantum Sci. Technol.* **2018**, *3*, 024009. [CrossRef]
60. Kivioja, J.M.; Nieminen, T.E.; Claudon, J.; Buisson, O.; Hekking, F.W.J.; Pekola, J.P. Observation of Transition from Escape Dynamics to Underdamped Phase Diffusion in a Josephson Junction. *Phys. Rev. Lett.* **2005**, *94*, 247002. [CrossRef]
61. Kivioja, J.M.; Nieminen, T.E.; Claudon, J.; Buisson, O.; Hekking, F.W.J.; Pekola, J.P. Weak coupling Josephson junction as a current probe: Effect of dissipation on escape dynamics. *New J. Phys.* **2005**, *7*, 179–179. [CrossRef]
62. Longobardi, L.; Massarotti, D.; Stornaiuolo, D.; Galletti, L.; Rotoli, G.; Lombardi, F.; Tafuri, F. Direct Transition from Quantum Escape to a Phase Diffusion Regime in YBaCuO Biepitaxial Josephson Junctions. *Phys. Rev. Lett.* **2012**, *109*, 050601. [CrossRef]

63. Bae, M.H.; Sahu, M.; Lee, H.J.; Bezryadin, A. Multiple-retrapping processes in the phase-diffusion regime of high-T_c intrinsic Josephson junctions. *Phys. Rev. B* **2009**, *79*, 104509. [CrossRef]
64. Yu, H.F.; Zhu, X.B.; Peng, Z.H.; Tian, Y.; Cui, D.J.; Chen, G.H.; Zheng, D.N.; Jing, X.N.; Lu, L.; Zhao, S.P.; et al. Quantum Phase Diffusion in a Small Underdamped Josephson Junction. *Phys. Rev. Lett.* **2011**, *107*, 067004. [CrossRef]
65. Massarotti, D.; Longobardi, L.; Galletti, L.; Stornaiuolo, D.; Montemurro, D.; Pepe, G.; Rotoli, G.; Barone, A.; Tafuri, F. Escape dynamics in moderately damped Josephson junctions. *Low Temp. Phys. Fiz. Nizk. Temp.* **2012**, *38*, 336.
66. Castellano, G.; Torrioli, G.; Chiarello, F.; Cosmelli, C.; Carelli, P. Return current in hysteretic Josephson junctions: Experimental distribution in the thermal activation regime. *J. Appl. Phys.* **1999**, *86*, 6405. [CrossRef]
67. Fenton, J.C.; Warburton, P.A. Monte Carlo simulations of thermal fluctuations in moderately damped Josephson junctions: Multiple escape and retrapping, switching- and return-current distributions, and hysteresis. *Phys. Rev. B* **2008**, *78*, 054526. [CrossRef]
68. Yoon, Y.; Gasparinetti, S.; Pekola, M.M.J.P. Capacitively Enhanced Thermal Escape in Underdamped Josephson Junctions. *J. Low Temp. Phys.* **2011**, *163*, 164. [CrossRef]
69. Martinis, J.M.; Devoret, M.H.; Clarke, J. Experimental tests for the quantum behavior of a macroscopic degree of freedom: The phase difference across a Josephson junction. *Phys. Rev. B* **1987**, *35*, 4682–4698. [CrossRef]